

1 Magnetospheric chaos and dynamical complexity response during storm time disturbance

2 Irewola Aaron Oludehinwa¹, Olasunkanmi Isaac Olusola¹, Olawale Segun Bolaji^{1,2}, Olumide
3 Olayinka Odeyemi¹, Abdullahi Ndzi Njah¹

4 ¹Department of Physics, University of Lagos, Nigeria

5 ²Department of Physics, University of Tasmania, Australia

6 Abstract

7 In this study, we examine the magnetospheric chaos and dynamical complexity response to the
8 disturbance storm time (D_{st}) and solar wind electric field (VB_s) during different categories of
9 geomagnetic storm (minor, moderate and major geomagnetic storm). The time series data of the
10 D_{st} and VB_s are analyzed for the period of nine years using nonlinear dynamics tools (Maximal
11 Lyapunov Exponent, MLE, Approximate Entropy, ApEn and Delay Vector Variance, DVV). We
12 found a significant trend between each nonlinear parameter and the categories of geomagnetic
13 storm. The MLE and ApEn values of the D_{st} indicate that chaotic and dynamical complexity
14 responses are high during minor geomagnetic storms, reduce at moderate geomagnetic storms and
15 decline further during major geomagnetic storms. However, the MLE and ApEn values obtained
16 from VB_s indicate that chaotic and dynamical complexity response are high with no significant
17 difference between the periods that are associated with minor, moderate and major geomagnetic
18 storms. The test for nonlinearity in the D_{st} time series during major geomagnetic storm reveals the
19 strongest nonlinearity features. Based on these findings, the dynamical features obtained in the
20 VB_s as input and D_{st} as output of the magnetospheric system suggest that the magnetospheric
21 dynamics is nonlinear and the solar wind dynamics is consistently stochastic in nature.

22 **Keywords:** D_{st} signals, Solar wind electric field (VB_s) signals, Geomagnetic storm, Chaotic
23 behaviour, Dynamical complexity, Nonlinearity.

24

25 **1.0 Introduction**

26 The response of chaos and dynamical complexity behaviour with respect to magnetospheric
27 dynamics varies. This is due to changes in the interplanetary electric fields imposed on the
28 magnetopause and those penetrating the inner magnetosphere and sustaining convection thereby
29 initiating geomagnetic storm (Pavlos et al. 1992). A prolonged southward turning of interplanetary
30 magnetic field (IMF, B_z), which indicates that solar wind-magnetosphere coupling is in-progress
31 was confirmed on many occasions for which such geomagnetic storm was driven by Corotating
32 Interaction Regions (CIRs), or by the sheath preceding an interplanetary coronal mass ejection
33 (ICME) or by a combination of the sheath and an ICME magnetic cloud (Russell et al. 1974;
34 Burton et al. 1975; Gonzalez and Tsurutani, 1987; Tsurutani et al. 1988; Cowley, 1995; Tsutomu,
35 2002; Yurchyshyn et al. 2004; Kozyra et al. 2006; Echer et al. 2008; Meng et al. 2019; Tsurutani
36 et al. 2020). Notably, the introduction of Disturbance Storm Time (D_{st}) index (Sugiura, 1964;
37 Sugiura and Kamei, 1991) unveil the quantitative measure of the total energy of the ring current
38 particles. Therefore, the D_{st} index remains one of the most popular global indicators that can
39 precisely reveal the severity of a geomagnetic storm (Dessler and Parker, 1959).

40 The D_{st} fluctuations exhibit different signatures for different categories of geomagnetic storm.
41 Ordinarily, one can easily anticipate that fluctuations in a D_{st} signal appear chaotic and complex.
42 These may arise from the changes in the interplanetary electric fields driven by the solar wind-
43 magnetospheric coupling processes. At different categories of geomagnetic storm, fluctuations in
44 the D_{st} signals differ (Oludehinwa et al. 2018). One obvious reason is that as the intensity of the
45 geomagnetic storm increases, the fluctuation behaviour in the D_{st} signal becomes more complex
46 and nonlinear in nature. It has been established that the electrodynamic response of the
47 magnetosphere to solar wind driver are non-autonomous in nature (Price and Prichard, 1993; Price

48 et al. 1994; Johnson and Wings, 2005). Therefore, the chaotic analysis of the magnetospheric time
49 series must be related to the concept of input-output dynamical process. Consequently, it is
50 necessary to examine the chaotic behaviour of the solar wind electric field (VB_s) as input signals
51 and the magnetospheric activity index (D_{st}) as output during different categories of geomagnetic
52 storms.

53 Several works have been presented on the chaotic and dynamical complexity behaviour of the
54 magnetospheric dynamics based on autonomous concept, i.e using the time series data of
55 magnetospheric activity alone such as auroral electrojet (AE), Amplitude Lower (AL) and D_{st}
56 index (Vassiliadis et al.1990; Baker and Klimas, 1990; Vassiliadis et al.1991; Shan et al. 1991;
57 Pavlos et al. 1994; Klimas et al. 1996; Valdivia et al. 2005; Mendes et al. 2017; Consolini, 2018).
58 They found evidence of low-dimensional chaos in the magnetospheric dynamics. For instance, the
59 report by Vassiliadis et al. (1991) shows that the computation of Lyapunov exponent for AL index
60 time series gives a positive value of Lyapunov exponent indicating the presence of chaos in the
61 magnetospheric dynamics. Unnikrishnan, (2008) studied the deterministic chaotic behaviour in the
62 magnetospheric dynamics under various physical conditions using AE index time series and found
63 that the seasonal mean value of Lyapunov exponent in winter season during quiet periods ($0.7 \pm$
64 0.11 min^{-1}) is higher than that of the stormy periods ($0.36 \pm 0.09 \text{ min}^{-1}$). Balasis et al. (2006)
65 examined the magnetospheric dynamics in the D_{st} index time series from pre-magnetic storm to
66 magnetic storm period using fractal dynamics. They found that the transition from anti-persistent
67 to persistent behaviour indicates that the occurrence of an intense geomagnetic storm is imminent.
68 Balasis et al. (2009) further reveal the dynamical complexity behaviour in the magnetospheric
69 dynamics using various entropy measures. They reported a significant decrease in dynamical
70 complexity and an accession of persistency in the D_{st} time series as the magnetic storm

71 approaches. Recently, Oludehinwa et al. (2018) examined the nonlinearity effects in D_{st} signals
72 during minor, moderate and major geomagnetic storm using recurrence plot and recurrence
73 quantification analysis. They found that the dynamics of the D_{st} signal is stochastic during minor
74 geomagnetic storm periods and deterministic as the geomagnetic storm increases.

75 Also, studies describing the solar wind and magnetosphere as non-autonomous system have been
76 extensively investigated. Price et al. (1994) examine the nonlinear input-output analysis of AL
77 index and different combinations of interplanetary magnetic field (IMF) with solar wind
78 parameters as input function. They found that only a few of the input combinations show any
79 evidence whatsoever for nonlinear coupling between the input and output for the interval
80 investigated. Pavlos et al. (1999) presented further evidence of magnetospheric chaos. They
81 compared the observational behaviour of the magnetospheric system with the results obtained by
82 analyzing different types of stochastic and deterministic input-output systems and asserted that a
83 low dimensional chaos is evident in magnetospheric dynamics. Devi et al. (2013) studied the
84 magnetospheric dynamics using AL index with the southward component of IMF, (B_z) and
85 observed that the magnetosphere and turbulent solar wind have values corresponding to nonlinear
86 dynamical system with chaotic behaviour. The modeling and forecasting approach have been
87 applied to magnetospheric time series using nonlinear models (Valdivia et al. 1996; Vassiliadis et
88 al. 1999; Vassiliadis, 2006; Balikhin et al. 2010). These efforts have improved our understanding
89 with regards to the facts that nonlinear dynamics can reveal some hidden dynamical information
90 in the observational time series. In addition to these nonlinear effects in D_{st} signals, a measure of
91 the exponential divergence and convergence within the trajectories of a phase space known as
92 Maximal Lyapunov Exponent (MLE), which has the potential to depict the chaotic behavior in the
93 D_{st} and VB_s time series during a minor, moderate and major geomagnetic storm have not been

94 investigated. In addition, to the best of our knowledge, computation of Approximate Entropy
95 (ApEn) that depicts the dynamical complexity behaviour during different categories of
96 geomagnetic storm has not been reported in the literature. The test for nonlinearity through delay
97 vector variance (DVV) analysis that establishes the degree at which nonlinearity response in D_{st}
98 time series during minor, moderate and major geomagnetic storms is not well known. It is worth
99 to note that understanding the dynamical characteristics in the D_{st} and VB_s signals at different
100 categories of geomagnetic storms will provide useful diagnostic information to different conditions
101 of space weather phenomenon. Consequently, this study attempts to carry out comprehensive
102 numerical analysis to unfold the chaotic and dynamical complexity behaviour in the D_{st} and VB_s
103 signals during minor, moderate and major geomagnetic storm. In section 2, our methods of data
104 acquisition are described. Also, the nonlinear analysis that we employed in this investigation are
105 detailed. In section 3, we unveiled our results and engage the discussion of results in section 5.

106 **2.0 Description of the Data and Nonlinear Dynamics**

107 The D_{st} index is derived by measurements from ground-based magnetic stations at low-latitudes
108 observatories around the world and depicts mainly the variation of the ring current, as well as the
109 Chapman-Ferraro Magnetopause currents, and tail currents to a lesser extent (Sugiura, 1964; Love
110 and Gannon, 2009). Due to its global nature, D_{st} time series provides a measure of how intense a
111 geomagnetic storm was (Dessel and Parker, 1959). In this study, we considered D_{st} data for the
112 period of nine years from January to December between 2008 and 2016 which were downloaded
113 from the World Data Centre for Geomagnetism, Kyoto, Japan ([http://wdc.kugi-kyoto-](http://wdc.kugi-kyoto-u.ac.jp/Dstae/index.html)
114 [u.ac.jp/Dstae/index.html](http://wdc.kugi-kyoto-u.ac.jp/Dstae/index.html)). The sampling time of D_{st} and VB_s time series data was 1-hour. We use
115 the classification of geomagnetic storms as proposed by Gonzalez et al. (1994) such that D_{st} index
116 value in the ranges $0 \leq Dst \leq -50nT$, $-50nT \leq Dst \leq -100nT$, $-100nT \leq Dst \leq -250nT$

117 are classified as minor, moderate and major geomagnetic storms respectively and each month is
118 being classified based on its minimum Dst value. The solar wind electric field (VB_s) data are
119 archived from the National Aeronautics and Space Administration, Space Physics Facility
120 (<http://omniweb.gsfc.nasa.gov>). It is well known that the dynamics of the solar wind contribute to
121 the driving of the magnetosphere (Burton et al. 1975). Furthermore, we took the solar wind electric
122 field (VB_s) as the input signal (Price and Prichard, 1993; Price et al. 1994). The VB_s was
123 categorized according to the periods of minor, moderate and major geomagnetic storm. Then, the
124 D_{st} and VB_s time series were subjected to a variety of nonlinear analytical tools explained as
125 follow:

126 **2.1 Phase Space Reconstruction and Observational time series**

127 An observational time series can be defined as a sequence of scalar measurements of some
128 quantity, which is a function of the current state of the system taken at multiples of a fixed sampling
129 time. In nonlinear dynamics, the first step in analyzing an observational time series data is to
130 reconstruct an appropriate state space of the system. Takens, (1981) and Mane, (1981) stated that
131 one time series or a few simultaneous time series are converted to a sequence of vectors. This
132 reconstructed phase space has all the dynamical characteristic of the real phase space provided the
133 time delay and embedding dimension are properly specified.

$$134 \quad X(t) = [x(t), x(t + \tau), x(t + 2\tau), \dots, x(t + (m - 1)\tau)]^T \quad (1)$$

135 where $X(t)$ is the reconstructed phase space, $x(t)$ is the original time series data, τ is the time
136 delay and m is the embedding dimension. An appropriate choice of τ and m are needed for the
137 reconstruction phase space which is determined by average mutual information and false nearest
138 neighbour respectively.

139 2.2 Average Mutual Information (AMI)

140 The method of Average Mutual Information (AMI) is one of the nonlinear techniques used to
141 determine the optimal time delay (τ) required for phase space reconstruction in observational time
142 series. The time delay mutual information was proposed by Fraser and Swinney, (1986) instead of
143 autocorrelation function. This method takes into account nonlinear correlations within the time
144 series data. It measures how much information can be predicted about one time series point, given
145 full information about the other. For instance, the mutual information between x_i and $x_{(i+\tau)}$
146 quantifies the information in state $x_{(i+\tau)}$ under the assumption that information at the state x_i is
147 known. The AMI for a time series, $x(t_i)$, $i = 1, 2, \dots, N$ is calculated as:

$$148 \quad I(T) = \sum_{x(t_i), x(t_i+T)} P(x(t_i), x(t_i + T)) \times \log_2 \left[\frac{P(x(t_i), x(t_i+T))}{P(x(t_i)) P(x(t_i+T))} \right] \quad (2)$$

149 Where $x(t_i)$ is the i th element of the time series, $T = k\Delta t$ ($k = 1, 2, \dots, k_{max}$), $P(x(t_i))$ is the
150 probability density at $x(t_i)$, $P(x(t_i), x(t_i + T))$ is the joint probability density at the pair
151 $x(t_i), x(t_i + T)$. The time delay (τ) of the first minimum of AMI is chosen as optimal time delay
152 (Fraser and Swinney, 1986). Therefore, the AMI was applied to the D_{st} and VB_S time series and
153 the plot of AMI against time delay is shown in Figure (3). We notice that the AMI showed the first
154 local minimum at roughly ($\tau = 15hr$). Furthermore, the values of τ near this value of ($\sim 15hr$)
155 maintain constancy for both VBs and D_{st} . In the analysis ($\tau = 15hr$) was used as the optimal
156 time delay for the computation of maximal Lyapunov exponent.

157

158

159

160 **2.3 False Nearest Neighbour (FNN)**

161 In determining the optimal choice of embedding dimension(m), the false nearest neighbour
 162 method was used in the study. It was suggested by Kennel et al. (1992). The concept is based on
 163 how the number of neighbours of a point along a signal trajectory changes with increasing
 164 embedding dimension. With increasing embedding dimension, the false neighbour will no longer
 165 be neighbours, therefore by examining how the number of neighbours changes as a function of
 166 dimension, an appropriate embedding dimension can be determined. For instance, suppose we
 167 have a one-dimensional time series. We can construct a time series $y(t)$ of D -dimensional points
 168 from the original one-dimensional time series $x(t)$ as follows:

169
$$y(t) = (x(t), x(t + \tau), \dots, x(t + (D - 1)\tau)) \quad (3)$$

170 where D is embedding dimension. Using the formular from Kennel et al. (1992); Wallot and
 171 Monster, (2018). If we have a D -dimensional phase space and denote the r th nearest neighbour of
 172 a coordinate vector $y(t)$ by $y^{(r)}(t)$, then the square of the Euclidean distance between $y(t)$ and
 173 the r th nearest neighbor is:

174
$$R_D^2(t, r) = \sum_{k=0}^{D-1} [x(t + k\tau) - x^{(r)}(t + k\tau)]^2 \quad (4)$$

175 Now applying the logic outlined above, we can go from a D -dimensional phase space to $(D + 1)$
 176 dimensional phase space by time-delay embedding, adding a new coordinate to $y(t)$, and ask what
 177 is the squared distance between $y(t)$ and the same r th nearest neighbour:

178
$$R_{D+1}^2(t, r) = R_D^2(t, r) + [x(t + D\tau) - x^{(r)}(t + D\tau)]^2 \quad (5)$$

179 As explained above, if the one-dimensional time series is already properly embedded in D
 180 dimensions, then the distance R between $y(t)$ and the r th nearest neighbour should not

181 appreciably change by some distance criterion R_{tol} (i. e $R < R_{tol}$). Moreover, the distance of the
182 nearest neighbour when embedded into the next higher dimension relative to the size of the
183 attractor should be less than some criterion A_{tol} (i. e $R_{D+1} < A_{tol}$). Doing this for the nearest
184 neighbour of each coordinate will result on many false nearest neighbours when embedding is
185 insufficient or in few (or no) false neighbours when embedding is sufficient. In the analysis, the
186 FNN was applied to the D_{st} and VB_s time series to detect the optimal value of embedding
187 dimension(m). Figure (4) shows a sample plot of the percentage of false nearest neighbour against
188 embedding dimension in one of the months under investigation (other months show similar results,
189 thus for brevity we depict only one of the results). We notice that the false nearest neighbor attains
190 its minimum value at $m \geq 5$ indicating that embedding dimension (m) from $m \geq 5$ are optimal
191 values. Therefore, $m = 5$ was used for the computation of maximal Lyapunov exponent.

192 **2.4 Maximal Lyapunov Exponent (MLE)**

193 The Maximal Lyapunov Exponent (MLE) is one of the most popular nonlinear dynamics tool used
194 for detecting chaotic behaviour in a time series data. It describes how small changes in the state of
195 a system grow at an exponential rate and eventually dominate the behaviour. An important
196 indication of chaotic behavior of a dissipative deterministic system is the existence of a positive
197 Lyapunov Exponent. A positive MLE signifies divergence of trajectories in one direction or
198 expansion of an initial volume in this direction. On the other hand, a negative MLE exponent
199 implies convergence of trajectories or contraction of volume along another direction. The
200 algorithm proposed by Wolf et al. (1985) for estimating MLE is employed to compute the chaotic
201 behavior of the D_{st} and VB_s time series at minor, moderate and major geomagnetic storm. Other
202 methods of determining MLE includes Rosenstein's method, Kantz's method and so on. In this
203 study, the MLE at minor, moderate and major geomagnetic storms periods was computed with

204 $m = 5$ and $\tau = 15hr$ as shown in figures 5 & 6 (bar plots) for D_{st} and VB_s . The calculation of
 205 MLE is explained as follows: given a sequence of vector $x(t)$, an m -dimensional phase space is
 206 formed from the observational time series through embedding theorem as

$$207 \quad \{x(t), x(t + \tau), \dots, x(t + (m - 1)\tau)\} \quad (6)$$

208 Where m and τ are as defined earlier, after reconstructing the observational time series, the
 209 algorithm locates the nearest neighbour (in Euclidean sense) to the initial point $\{x(t_0), \dots, x(t_0 +$
 210 $(m - 1)\tau\}$ and denote the distance between these two points $L(t_0)$. At a later point t_1 , the initial
 211 length will have evolved to length $L'(t_1)$. Then the MLE is calculated as:

$$212 \quad \lambda = \frac{1}{t_M - t_0} \sum_{k=1}^M \log_2 \frac{L'(t_k)}{L(t_{k-1})} \quad (7)$$

213 M is the total number of replacement steps. We look for a new data point that satisfies two criteria
 214 reasonably well: its separation, $L(t_1)$, from the evolved fiducial point is small. If an adequate
 215 replacement point cannot be found, we retain the points that were being used. This procedure is
 216 repeated until the fiducial trajectory has traversed the entire data

217 **2.5 Approximate Entropy (ApEn)**

218 Approximate Entropy (ApEn) measures the dynamical complexity in observational time series. It
 219 was proposed by Pincus, (1991), it provides a generalized measure of regularity, such that it
 220 accounts for the logarithm likelihood in the observational time series. For instance, a dataset of
 221 length, N , that repeat itself for m points within a boundary will again repeat itself for $m + 1$ points.
 222 Because of its computational advantage, ApEn has been widely used in many areas of disciplines
 223 to study dynamical complexity (Pincus and Kalman (2004); Pincus and Goldberger (1994);

224 McKinley et al. (2011); Kannathan et al. (2005); Balasis et al. (2009); Shujuan and Weidong,
 225 (2010); Moore and Marchant (2017)). The ApEn is computed using the formula below:

$$226 \quad ApEn(m, r, N) = \frac{1}{N-m+1} \sum_{i=1}^{N-m+1} \log C_i^m(r) - \frac{1}{N-m} \sum_{i=1}^{N-m} \log C_i^m(r) \quad (8)$$

227 where $C_i^m(r) = \frac{1}{N-m+1} \sum_{j=1}^{N-m+1} \Theta(r - \|x_i - x_j\|)$ is the correlation integral and r is the tolerance.

228 To compute the ApEn for the D_{st} and VB_s time series classified at minor, moderate and major
 229 geomagnetic storm from 2008 to 2016, we choose ($m = 3, \tau = 1hr$). We refer the works of
 230 Pincus, (1991); Kannathal et al. (2005); and Balasis et al. (2009) to interested readers where all
 231 the computational steps regarding ApEn were explained in details. Figures (5 & 6) depict the stem
 232 plots of ApEn for D_{st} and (VB_s) from 2008 to 2016.

233 **2.6 Delay Vector Variance (DVV) analysis**

234 The Delay Vector Variance (DVV) is a unified approach in analyzing and testing for nonlinearity
 235 in a time series (Gautama et al. 2004; Mandic et al. 2007). The basic idea of the DVV is that, if
 236 two delay vectors of a predictable signal are close to each other in terms of the Euclidean distance,
 237 they should have similar target. For instance, when a time delay (τ) is embedded into a time series
 238 $x(k)$, $k = 1, 2, \dots, N$, then a reconstructed phase space vector is formed which represents a set of
 239 delay vectors (DVs) of a given dimension.

$$240 \quad X(k) = [X_{k-m\tau}, \dots, X_{k-\tau}]^T \quad (9)$$

241 Reconstructing the phase space, a set (λ_k) is generated by grouping those DVs that are with a
 242 certain Euclidean distance to DVs ($X(k)$). For a given embedding dimension (m), a measure of
 243 unpredictability σ^{*2} is computed over all pairwise Euclidean distance between delay vector as

$$244 \quad d(i, j) = \|x(i) - x(j)\| \quad (i \neq j) \quad (10)$$

245 Then, sets $\lambda_k(r_d)$ are generated as the sets which consist of all delay vectors that lie closer to $x(k)$
 246 than a certain distance r_d .

$$247 \quad \lambda_k(r_d) = \{x(i) \mid \|x(k) - x(i)\| \leq r_d\} \quad (11)$$

248 For every set $\lambda_k(r_d)$, the variance of the corresponding target $\sigma^{*2}(r_d)$ is

$$249 \quad \sigma^{*2}(r_d) = \frac{\frac{1}{N} \sum_{k=1}^N \sigma_k^2(r_d)}{\sigma_k} \quad (12)$$

250 where $\sigma^{*2}(r_d)$ is target variance against the standardized distance indicating that Euclidean
 251 distance will be varied in a manner standardized with respect to the distribution of pairwise
 252 distance between DVs. Iterative Amplitude Adjusted Fourier Transform (IAAFT) method is used
 253 to generate the surrogate time series (Kugiumtzis, 1999). If the surrogate time series yields DV
 254 plots similar to the original time series and the scattered plot coincides with the bisector line, then
 255 the original time series can be regarded as linear (Theiler et al. 1992; Gautama et al. 2004; Imitaz,
 256 2010; Jaksic et al. 2016). On the other hand, if the surrogate time series yield DV plot that is not
 257 similar to that of the original time series, then the deviation from the bisector lines indicates
 258 nonlinearity. The deviation from the bisector lines grows as a result of the degree of nonlinearity
 259 in the observational time series.

$$260 \quad t^{D_{VV}} = \sqrt{\langle (\sigma^{*2}(r_d) - \frac{\sum_{i=1}^N \sigma_{s,i}^{*2}}{N_s}) \rangle} \quad (13)$$

261 where $\sigma_{s,i}^{*2}(r_d)$ is the target variance at the span r_d for the i^{th} surrogate. To carry out the test for
 262 nonlinearity in the D_{st} signals, $m = 3$ and $n_d = 3$, the number of references DVs=200, and
 263 number of surrogates, $N_s = 25$ was used in all the analysis. Then we examined the nonlinearity
 264 response at minor, moderate and major geomagnetic storm.

265 3.0 Results

266 In this study, D_{st} and VB_s time series from January to December was analyzed for the period of
267 nine years (2008 to 2016) to examine the chaotic and dynamical complexity response in the
268 magnetospheric dynamics during the month of minor, moderate and major geomagnetic storms
269 activity. Figures (1) & (2), display the samples of fluctuation signatures of D_{st} and VB_s signals
270 classified as (a): the month of minor, (b): the month of moderate and (c): the month of major
271 geomagnetic storm activity. The plot of Average Mutual information against time delay (τ) shown
272 in Figure (3) depicts that the first local minimum of the AMI function was found to be roughly at
273 $\tau = 15$ hr. Furthermore, we notice that the values of τ near this value of (~ 15 hr) maintain constancy
274 for both VB_s and D_{st} . Also, in Figure (4), we display the plot of the percentage of false nearest
275 neighbour against embedding dimension (m). It is obvious that a decrease in false nearest
276 neighbour when increasing the embedding dimension drop steeply to zero at the optimal
277 dimension ($m = 5$), thereafter the false neighbours stabilizes at $m = 5$ for VB_s and D_{st} . Therefore,
278 $m = 5$ and $\tau = 15$ hr was used for the computation of MLE at different categories of geomagnetic
279 storm, while $m = 3$ and $\tau = 1$ hr are applied for the computation of ApEn values.

280 The results of MLE (bar plot) and ApEn (stem plot) for D_{st} at the month of minor, moderate and
281 major geomagnetic storms activity are shown in Figure 5. During the month of minor geomagnetic
282 storms activity, we notice that the value of MLE ranges between 0.07 and 0.14 for most of the
283 months classified as minor geomagnetic storm. Similarly, the ApEn (stem plot) ranges between
284 0.59 and 0.83. It is obvious that strong chaotic behaviour with high dynamical complexity are
285 associated with minor geomagnetic storms. During the month of moderate geomagnetic storm
286 activity, (see b part of Figure (5)), we observe a reduction in MLE values (0.04~0.07) compared
287 to minor geomagnetic storm periods. Within the observed values of MLE during the month of

288 moderate geomagnetic storms activity, we found a slight rise of MLE in the following months
289 (Mar 2008), (Apr 2011), (Jan 2012, Feb 2012, Apr 2012), (Jul 2015, Aug 2015, Sept 2015,
290 Oct2015, Nov 2015) and (Nov 2016). Also, the ApEn revealed a reduction in values between 0.44
291 and 0.57 at the month of moderate geomagnetic storms activity. The lowest values of ApEn were
292 noticed in the following months: May 2010, Mar 2011, and Jan 2016. During major geomagnetic
293 storm as shown in Figure 5, the minimum and maximum value of MLE is respectively 0.03 and
294 0.04 implying a very strong reduction of chaotic behaviour compared with the month of minor and
295 moderate geomagnetic storm activity. The lowest values of MLE were found in the months of Jul
296 2012, Jun 2013 and Mar 2015. Interestingly, further reduction in ApEn value (0.29~0.40) was as
297 well noticed during this period. Thus, during the month of major geomagnetic storm activity,
298 chaotic behaviour and dynamical complexity subsides significantly.

299 We display in Figure 6, the results of MLE and ApEn computation for the VB_s which has been
300 categorized according to the month of minor, moderate and major geomagnetic storm activity. The
301 values of MLE (bar plot) were between 0.06 and 0.20 for VB_s . The result obtained indicate strong
302 chaotic behaviour with no significant difference in chaoticity during minor, moderate and major
303 geomagnetic storm. Similarly, the results obtained from computation of ApEn (stem plot) for VB_s
304 depict a minimum value of 0.60 and peak value of 0.87 as shown in Figure 6. The ApEn values of
305 VB_s indicates high dynamical complexity response with no significant difference during the
306 periods of the three categories of geomagnetic storm investigated.

307 The test for nonlinearity in the D_{st} signals during the month of minor, moderate and major
308 geomagnetic storms activity was analyzed through the DVV analysis. Shown in Figure 9 is the
309 DVV plot and DVV scatter plot during minor geomagnetic storm for January 2009 and January
310 2014. We found that the DVV plots during the month of minor geomagnetic storms activity reveal

311 a slight separation between the original and surrogate data. Also, the DVV scatter plots shows a
312 slight deviation from the bisector line between the original and surrogate data which implies
313 nonlinearity. Also, during the month of moderate geomagnetic storm activity, we notice that the
314 DVV plot depicts a wide separation between the original and the surrogate data. Also, a large
315 deviation from the bisector line between the original and the surrogate data was also observed in
316 the DVV scatter plot as shown in Figure (8) thus indicating nonlinearity. In Figure (9), we display
317 samples of DVV plot and DVV scatter plot during major geomagnetic storm for Oct 2011 and Dec
318 2015. The original and the surrogate data showed a very large separation in the DVV plot during
319 the month of major geomagnetic storm activity. While the DVV scatter plot depict a very large
320 deviation from the bisector line between the original and the surrogate data which is also an
321 indication of nonlinearity. The DVV analysis of the VB_s time series during the month of minor,
322 moderate and major geomagnetic storm activity shown in Figures (10-12) revealed a slight
323 separation between the original and surrogate data with no significant difference between the
324 month of minor, moderate and major geomagnetic activity.

325 **4.0 Discussion of Results**

326 **4.1 The chaotic and dynamical complexity response in D_{st} during the months of minor,** 327 **moderate and major geomagnetic storms**

328 Our result shows that the values of MLE for D_{st} during the month of minor geomagnetic storm
329 activity are higher, indicating significant chaotic response during minor geomagnetic stormy
330 periods (see the bar plots in Figure 5). This increase in chaotic behaviour for D_{st} signals during
331 minor geomagnetic storm may be as a result of asymmetry features in the longitudinal distribution
332 of solar source region for the Corotating Interaction Regions (CIR) signatures responsible for the
333 development of geomagnetic storms (Turner et al. 2006; Kozyra et al. 2006). CIR generated

334 magnetic storms are generally weaker than ICME/MC generated storms (Richardson and Cane,
335 2011). Therefore, we suspect that the increase in chaotic behaviour during minor geomagnetic
336 storm is strongly associated with the asymmetry features in the longitudinal distribution of solar
337 source region for the Corotating Interaction Regions (CIR) signatures. For most of these periods
338 of moderate geomagnetic storms, the values of MLE decreases compared to the month of minor
339 geomagnetic storms activity. This revealed that as geomagnetic stormy events build up, the level
340 of unpredictability and sensitive dependence on initial condition (chaos) begin to decrease
341 (Lorentz, 1963; Stogaz, 1994). The chaotic behaviour during the month of major geomagnetic
342 storm decreases significantly compared with the month of moderate geomagnetic storm activity.
343 The reduction in chaotic response during the month of moderate and its further declines at major
344 geomagnetic storm activity may be attributed to the disturbance in the interplanetary medium
345 driven by sheath preceding an interplanetary coronal mass ejection (ICME) or combination of the
346 sheath and an ICME magnetic cloud (Echer et al. 2008; Tsurutani et al. 2003; Meng et al. 2019).
347 Notably, the dynamics of the solar wind-magnetospheric interaction are dissipative chaotic in
348 nature (Pavlos, 2012); and, the electrodynamic of the magnetosphere due to the flux of
349 interplanetary electric fields had a significant impact on the state of the chaotic signatures. For
350 instance, the observation of strong chaotic behaviour during the month of minor geomagnetic
351 storm activity suggests that the dynamics was characterized by a weak magnetospheric
352 disturbance. While the reduction in chaotic behaviour at moderate and major geomagnetic storm
353 period reveals the dynamical features with regards to when a strong magnetospheric disturbance
354 begins to emerge. Therefore, our observation of chaotic signatures at different categories of
355 geomagnetic storm has potential capacity to give useful diagnostic information about monitoring
356 space weather events. It is important to note that the features of D_{st} chaotic behaviour at different

357 categories of geomagnetic storm has not been reported in the literature to the best of our
358 knowledge. For example, previous study of Balasis et al. (2009, 2011) investigate dynamical
359 complexity behaviour using different entropy measures and revealed the existence of low
360 dynamical complexity in the magnetospheric dynamics and attributed it to ongoing large
361 magnetospheric disturbance (major geomagnetic storm). The work of Balasis et al. (2009, 2011)
362 where certain dynamical characteristic evolved in the D_{st} signal was limited to one year data
363 (2001). It is worthy to note that the year 2001, according to sunspot variations is a period of high
364 solar activity during solar cycle 23. It is characterized by numerous and strong solar eruptions that
365 were followed by significant magnetic storm activities. This confirms that on most of the days in
366 year 2001, the geomagnetic activity is strongly associated with major geomagnetic storm. The
367 confirmation of low dynamical complexity response in the D_{st} signal during major geomagnetic
368 storm agree with our current study. However, the idea of comparing the dynamical complexity
369 behaviour at different categories of geomagnetic storm and reveal its chaotic features was not
370 reported. This is the major reason why our present investigation is crucial to the understanding of
371 the level of chaos and dynamical complexity involved during different categories of geomagnetic
372 storm. As an extension to the single-year investigation done by Balasis et al. (2009, 2011) during
373 a major geomagnetic storm, we further investigated nine years data of D_{st} that covered minor,
374 moderate and major geomagnetic storm (see Figure (5), stem plots) and unveiled their dynamical
375 complexity behaviour. During major geomagnetic stormy periods, we found that the ApEn values
376 decrease significantly, indicating reduction in the dynamical complexity behaviour. This is in
377 agreement with the low dynamical complexity reported by Balasis et al. (2009, 2011) during a
378 major geomagnetic period. Finally, based on the method of DVV analysis, we found that test of

379 nonlinearity in the D_{st} time series during major geomagnetic storm reveals the strongest
380 nonlinearity features.

381 **4.2 The chaotic and dynamical complexity behaviour in the VB_s as input signals.**

382 The results of the MLE values for VB_s revealed a strong chaotic behaviour during the three
383 categories of geomagnetic storm. Comparing these MLE values during the month of minor to those
384 observed during moderate and major geomagnetic storm activity, the result obtained did not
385 indicate any significant difference in chaoticity (bar plots, Figure (6)). Also, the ApEn values of
386 VB_s during the periods associated with minor, moderate and major geomagnetic storm revealed
387 high dynamical complexity behaviour with no significant difference between the three categories
388 of geomagnetic storm investigated. These observations of high chaotic and dynamical complexity
389 behaviour in the dynamics of VB_s may be due to interplanetary discontinuities caused by the abrupt
390 changes in the interplanetary magnetic field direction and plasma parameters (Tsurutani et al.
391 2010). Also, the indication of high chaotic and dynamical complexity behaviour in VB_s signifies
392 that the solar wind electric field is stochastic in nature. The DVV analysis for VB_s revealed
393 nonlinearity features with no significant difference between the month of minor, moderate and
394 major geomagnetic storm activity. It is worth mentioning that the dynamical complexity behaviour
395 for VB_s is different from what was observed for D_{st} time series data. For instance, our results for
396 D_{st} times series revealed that the chaotic and dynamical complexity behaviour of the
397 magnetospheric dynamics are high during minor geomagnetic storm, reduce at moderate
398 geomagnetic storm and further decline during major geomagnetic storm. While the VB_s signal
399 revealed a high chaotic and dynamical complexity behaviour at all the categories of geomagnetic
400 storm period. Therefore, these dynamical features obtained in the VB_s as input signal and the D_{st}
401 as the output in describing the magnetosphere as a non-autonomous system further support the

402 finding of Donner et al. (2019) that found increase or no change in dynamical complexity
403 behaviour for VB_s and low dynamical complexity behaviour during storm using recurrence
404 method. Thus, suggesting that the magnetospheric dynamics is nonlinear and the solar wind
405 dynamics is consistently stochastic in nature.

406 **5.0 Conclusions**

407 This work has examined the magnetospheric chaos and dynamical complexity behaviour in the
408 disturbance storm time (D_{st}) and solar wind electric field (VB_s) as input during different categories
409 of geomagnetic storm. The chaotic and dynamical complexity behaviour during the month of
410 minor, moderate and major geomagnetic storm activity for solar wind electric field (VB_s) as input
411 and D_{st} as output of the magnetospheric system were analyzed for the period of 9 years using
412 nonlinear dynamics tools. Our analysis has shown a noticeable trend of these nonlinear parameters
413 (MLE and ApEn) and the categories of geomagnetic storm (minor, moderate and major). The MLE
414 and ApEn values of the D_{st} have indicated that the chaotic and dynamical complexity behaviour
415 are high during the month of minor geomagnetic storm, low during moderate geomagnetic storm
416 and further reduced during major geomagnetic storm activity. The values of MLE and ApEn
417 obtained from VB_s indicate that chaotic and dynamical complexity are high with no significant
418 difference during the periods of minor, moderate and major geomagnetic storm. Finally, the test
419 for nonlinearity in the D_{st} time series during major geomagnetic storm reveals the strongest
420 nonlinearity features. Based on these findings, the dynamical features obtained in the VB_s as input
421 and D_{st} as output of the magnetospheric system suggest that the magnetospheric dynamics is
422 nonlinear and the solar wind dynamics is consistently stochastic in nature.

423

424 **7.0 Acknowledgement**

425 The authors would like to acknowledge the World Data Centre for Geomagnetism, Kyoto, and the
426 National Aeronautics and Space Administration, Space Physics Facility (NASA) for making the
427 Dst data and solar wind plasma data available for research purpose.

428 **Declaration of Interest statement**

429 The authors declare that there is no conflict of interest.

430 **References**

431 Baker, D.N., Klimas, A.J., (1990). The evolution of weak to strong geomagnetic activity: An
432 interpretation in terms of deterministic chaos. *J. GeoPhys. Res. Letts.* Vol. 17, No. 1, PP. 41-
433 44.

434 Balasis, G., Daglis, I.A., Anastasiadia, A., Eftaxias, K., (2011). Detection of dynamical complexity
435 changes in Dst time series using entropy concepts and rescaled range analysis. W.Liu, M.
436 Fujimoto (eds.), *The Dynamics Magnetosphere*, IAGA Special Sopron Book Series 3, doi:
437 10.1007/978-94-007-0501-2_12, Springer Science+Business Media B.V. 2011.

438 Balasis, G., I.A. Daglis, C. Papadimitriou, M. Kalimeri, A. Anastasiadis, K. Eftaxias (2009).
439 Investigating dynamical complexity in the magnetosphere using various entropy measures,
440 *J.Geophys.Res.*, 114, A0006, doi: 10.1029/2008JA 014035.

441 Balasis, G., I.A. Daglis, P. Kapis, M.Mandea, D. Vassiliadis, K. Eftaxias (2006). From pre-storm
442 activity to magnetic storms: a transition described in terms of fractal dynamics, *Ann.Geophys.*,
443 24, 3557-3567, www.ann-geophys.net/24/3557/2006.

444 Balikhin, M.A., Boynton, R.J., Billings, S.A., Gedalin, M., Ganushkina, N., Coca, D., (2010). Data
445 based quest for solar wind-magnetosphere coupling function, *Geophys.Res.Lett*, 37, L24107,
446 doi: 10.1029/2010GL045733.

447 Burton, R.K., McPherron, R.L., Russell, C.T., (1975). An empirical relationship between
448 interplanetary conditions and Dst. *Journal of Geophysical Research*, Vol.80, No.31.

449 Consolini, G., (2018), Emergence of dynamical complexity in the Earth's magnetosphere, *Machine*
450 *learning techniques for space weather*, PP. 177-202, doi: 10.1016/B978-0-12-811788-0.00007-
451 X

452 Cowley, S.W.H., (1995). The earth's magnetosphere: A brief beginner's guide, *EOS*
453 *Trans.Am.GeoPhys.Union*, 76, 525.

454 Dessler, A.J., Parker, E.N., (1959). Hydromagnetic theory of magnetic storm. *J. GeoPhys. Res*, 64,
455 PP 2239-2259.

456 Devi, S.P., Singh, S.B., Sharma, A.S., (2013). Deterministic dynamics of the magnetosphere:
457 results of the 0-1 test. *Nonlin. Processes Geophys.*, 20, 11-18, 2013, [www.nonlin-processes-](http://www.nonlin-processes-geophys.net/20/11/2013)
458 [geophys.net/20/11/2013](http://www.nonlin-processes-geophys.net/20/11/2013), doi: 10. 5194/npg-20-11-2013.

459 Donner, R.V., Balasis, G., Stolbova,V., Georgiou, M., Weiderman, M., Kurths, J. (2019).
460 Recurrence-based quantification of dynamical complexity in the earth's magnetosphere at
461 geospace storm time scales. *Journal of Geophysical Research: Space Physics*, 124, 90-108,
462 doi: 10.1029/2018JA025318.

463 Echer, E., Gonzalez, D., Alves, M.V., (2006). On the geomagnetic effects of solar wind
464 interplanetary magnetic structures. Space Weather, Vol.4, S06001,
465 doi:10.1029/2005SW000200.

466 Echer, E., Gonzalez, W.D., Tsurutani, B.T., Gonzalez, A. L. C., (2008), Interplanetary conditions
467 causing intense geomagnetic storms ($D_{st} \leq -100nT$) during solar cycle 23 (1996–2006), J.
468 Geophys. Res., 113, A05221, doi:10.1029/2007JA012744.

469 Fraser, A.M., (1986). Using mutual information to estimate metric entropy, dimension and
470 entropies in chaotic system, Springer-Verlag, 1986, PP: 82-91.

471 Fraser, A.M., Swinney, H.L., (1986). Independent coordinates for strange attractors from mutual
472 information, Phys.Rev.A 33, 1134-1140.

473 Gautama, T., Mandic, D.P., Hulle, M.M.V., (2004). The delay vector variance method for detecting
474 determinism and nonlinearity in time series. Physica D, 190, 167-176, doi:
475 10.1016/j.physd.2003.11.001.

476 Gonzalez, W.D., Joselyn, J.A., Kamide, Y., Kroehl, H.W., Rostoker, G., Tsurutani, B.T.,
477 Vasyliunas, V.M., (1994). What is a geomagnetic storm? J. Geophys. Res.: Space Physics,
478 Vol. 99, issue A4, pg. 5771-5792, doi: 10.1029/93JA02867.

479 Gonzalez, W.D., Tsurutani, B.T., (1987). Criteria of interplanetary parameters causing intense
480 magnetic storm ($D_{st} < -100nT$). Planetary and Space Science,
481 <https://ntrs.nasa.gov/search.jsp?R=198800068>.

482 Horne, R.H., Glauert, S.A., Meredith, N.P., Boscher, D., Maget, V., Heynderickx, D., and Pitford,
483 D. (2013). Space weather impacts on satellites and forecasting the Earth's electron radiation
484 belts with SPACECAST. *Space weather*, **11**, 169 - 186

485 Imtiaz, A., (2010). Detection of nonlinearity and stochastic nature in time series by delay vector
486 variance method, *International journal of Engineering & Technology*, Vol. 10, No. 02.

487 Jaksic, V., Mandic, D.P., Ryan, K., Basu, B., Pakrashi V., (2016). A Comprehensive Study of the
488 Delay Vector Variance Method for Quantification of Nonlinearity in dynamical Systems.
489 *R.Soc.OpenSci.*, 2016: 3:150493, <http://dx.doi.org/10.1098/rsos.150493>.

490 Johnson, J.R., Wing, S., (2005), A solar cycle dependence of nonlinearity in magnetospheric
491 activity. *J. Geophys. Res.*, 110, A04211, doi: 10.1029/2004JA010638.

492 Kannathal, N., M.L. Choo, U. R. Acharya, P. K. Sadasivan (2005). Entropies for detecting of
493 epilepsy in EEG, *Computer Methods and Programs in Biomedicine* (2005) 80, 187-194,
494 www.intl.elsevierhealth.com/journals/cmpb.

495 Kennel, M.B., R. Brown, H.D.I. Abarbanel (1992). Determining embedding dimension for phase-
496 space reconstruction using a geometrical construction, *PHYSICAL REVIEW A*, Volume 45,
497 Number 6.

498 Klimas, A.J., Vassiliadis, D., Baker, D.N., Roberts, D.A., (1996). The organized nonlinear
499 dynamics of the magnetosphere. *J. Geophys. Res.* Vol.101, No. A6, PP 13089-13113.

500 Kozyra, J.U., Crowley, G., Emery, B.A., Fang, X., Maris, G., Mlynczak, M.G., Niciejewski, R.J.,
501 Palo, S.E., Paxton, L.J., Randall, C.E., Rong, P.P., Russell, J.M., Skinner, W., Solomon, S.C.,
502 Talaat, E.R., Wu, Q., Yee, J.H., (2006), Response of the Upper/Middle Atmosphere to Coronal

503 Holes and Powerful High-Speed Solar Wind Streams in 2003, Geophysical Monograph Series
504 167, 10.1029/167GM24.

505 Kugiumtzis, D., (1999). Test your surrogate before you test your nonlinearity, Phys. Rev. E, 60,
506 2808-2816.

507 Lorenz, E.N., (1963). Determining nonperiodic flow. J. Atmos.Sci.,20,130.

508 Love, J.J., Gannon, J.L. (2009). Revised Dst and the epicycles of magnetic disturbance: 1958-2007.
509 Ann.GeoPhys., 27, 3101-3131.

510 Mandic, D.P., Chen, M., Gautama, T., Van Hull, M.M., Constantinides, A., (2007). On the
511 Characterization of the Deterministic/Stochastic and Linear/Nonlinear Nature of Time Series.
512 *Proc.R.Soc*, 2008: A464, 1141-1160, doi: 10.1098/rspa. 2007.0154.

513 Mane, R., (1981). On the dimension of the compact invariant sets of certain nonlinear maps, D.Rand
514 and L.S.Young, eds, 1981.

515 Mckinley, R.A., McIntire, L.K., Schmidt, R., Repperger, D.W., Caldwell, J.A., (2011). Evaluation
516 of Eye Metrics as a Detector of Fatigue. Human factor, 53 (4): 403-414, doi:
517 10.1177/0018720811411297.

518 Mendes, O., Dominques, M.O., Echer, E., Hajra, R., Menconi, V.E., (2017), Characterization of
519 high-intnesity, long-duration continuous auroral activity (HILDCAA) events using
520 recurrence quantification analysis. Nonlin. Processes Geophys.,24,407-417, doi:10.5194/npg-
521 24-407-2017.

522 Meng, X., Tsurutani, B. T., Mannucci, A. J. (2019). The solar and interplanetary causes of
523 superstorms (minimum $Dst \leq -250$ nT) during the space age. *Journal of Geophysical Research:*
524 *Space Physics*, 124, 3926–3948. <https://doi.org/10.1029/2018JA026425>.

525 Millan, H., Gharbarian-Alavijeh, B., Garcia-Fornaris, I., (2010). Nonlinear dynamics of mean daily
526 temperature and dewpoint time series at Babolsar, Iran, 1961-2005. Elsevier, *Atmospheric*
527 *Research* 98 (2010) 89-101, doi: 10.1016/j.atmosres.2010.06.001.

528 Moore, C., Marchant, T., (2017). The approximate entropy concept extended to three dimensions
529 for calibrated, single parameter structural complexity interrogation of volumetric images.
530 *Physics in Medicine & Biology*, 62(15).

531 Oludehinwa, I.A., Olusola, O.I., Bolaji, O.S., Odeyemi, O.O., (2018). Investigation of nonlinearity
532 effect during storm time disturbance, *Adv. Space. Res.*, 62 (2018) 440-456, doi:
533 10.1016/j.asr.2018.04.032.

534 Omkar, P.T., Verma, P.L., (2013). Solar features and solar wind plasma parameters with
535 geomagnetic storms during the period of 2002-2006. *Indian Journal of Applied Research*,
536 Vol.3, Issue.5, ISSN-2249-555X.

537 Pavlos, G.P., (1994). The magnetospheric chaos: a new point of view of the magnetospheric
538 dynamics. Historical evolution of magnetospheric chaos hypothesis the past two decades.
539 Conference Proceeding of the 2nd Panhellenic Symposium held in Democritus University of
540 Thrace, Greece, 26-29, April, edited 1994.

541 Pavlos, G.P., (2012). Magnetospheric dynamics and Chaos theory

542 Pavlos, G.P., Athanasiu, M.A., Diamantidis, D., Rigas, A.G., Sarri, E.T., (1999). Comments and
543 new results about the magnetospheric chaos hypothesis. *Nonlinear Processes in Geophysics*
544 (1999) 6: 99-127.

545 Pavlos, G.P., Rigas, A.G., Dialetis, D., Sarris, E.T., Karakatsanis, L.P., Tsonis, A.A., (1992).
546 Evidence of chaotic dynamics in the outer solar plasma and the earth magnetosphere. *Chaotic*
547 *dynamics: Theory and Practice*, Edited by T. Bountis, Plenum Press, New York, Page. 327-
548 339, doi:10.1007/978-1-4615-3464-8_30.

549 Pincus, S.M., (1991). Approximate entropy as a measure of system complexity, *Proc.Natl.Acad.Sci.*
550 *USA*, Vol.88, PP. 2297-2301.

551 Pincus, S.M., Goldberger, A.L., (1994). Physiological time series analysis: what does regularity
552 quantify, *The American Journal of Physiology*, 266 (4): 1643-1656.

553 Pincus, S.M., Kalman, E.K., (2004). Irregularity, volatility, risk, and financial market time series,
554 *Proceedings of the National Academy of Sciences*, 101 (38): 13709-13714, doi:
555 10.1073/pnas.0405168101.

556 Price, C.P., Prichard, D., Bischoff, J.E., (1994). Nonlinear input/output analysis of the auroral
557 electrojet index. *Journal of Geophysical Research*, Vol.99, No: A7, PP: 227-238.

558 Price,C.P., Prichard, D., (1993). The Non-linear response of the magnetosphere: 30 October, 1978.
559 *Geophysical Research Letters*, Vol.20.

560 Richardson, I.G., Cane, H.V., (2011), Geoeffectiveness (D_{st} and K_p) of interplanetary coronal
561 mass ejections during 1995-2009 and implication for storm forecasting, *Space Weather*, 9,
562 S07005, doi:10.1029/2011SW000670.

563 Russell, C.T., (2001). Solar wind and Interplanetary Magnetic Field: A Tutorial. Space Weather,
564 Geophysical Monograph 125, Page: 73-89.

565 Russell, C.T., McPherron, R.L., Burton, R.K. (1974). On the cause of geomagnetic storms,
566 J.GeoPhys.Res., 79, 1105-1109.

567 Shujuan G., Weidong, Z., (2010). Nonlinear feature comparison of EEG using correlation
568 dimension and approximate entropy, 3rd international conference on biomedical engineering
569 and informatics.

570 Strogatz, S.H., (1994), Nonlinear dynamics and chaos with Application to physics, Biology,
571 chemistry and Engineering, New York, John Wiley & Sons.

572 Sugiura, M. (1964). Hourly Values of equatorial Dst for the IGY, Ann.Int. GeoPhys. Year, 35, 9-
573 45.

574 Takens, F., (1981). Detecting Strange Attractors in Turbulence in Dynamical Systems, *D.Rand &*
575 *L.Young Eds*, 1981: 898, 366-381.

576 Theiler, J., Eubank, S., Longtin, A., Galdrikian, B., Farmer, J.D., (1992), Testing for nonlinearity
577 in time series: The method of surrogate data, *Physica D*, 58, 77.

578 Tsurutani, B.T., Gonzalez, W. D., Tang, F., Akasofu, S.I., Smith, E.J., (1988), Origin of
579 Interplanetary Southward Magnetic Fields Responsible for Major Magnetic Storms Near Solar
580 Maximum (1978-1979), *Journal of Geophysical Research*, Vol. 93, No. A8, Pages 8519-8531,
581 Paper number 7A9404, 0148-0227/88/007 A-9404\$05.00.

582 Tsurutani, B.T., Gonzalez, W.D., Lakhina, G.S. Alex, S., (2003). The extreme magnetic storm of
583 1-2 September 1859, *J. Geophys. Res.* 108(A7), doi: 10.1029/2002JA009504.

584 Tsurutani, B.T., Lakhina, G.S., Hajra, R., (2020), The physics of space weather/solar-terrestrial
585 physics (STP): what we know now and what the current and future challenges are, *Nonlin.*
586 *Processes Geophys.*, 27, 75–119, [doi:10.5194/npg-27-75-2020](https://doi.org/10.5194/npg-27-75-2020).

587 Tsurutani, B.T., Lakhina, G.S., Verkhoglyadova, O.P., Gonzalez, W.D., Echer, E., Guarnieri, F.L.,
588 (2010). A review of interplanetary discontinuities and their geomagnetic effects. *Journal of*
589 *Atmospheric and Solar-Terrestrial Physics*, doi: 10.1016/j.jastp.2010.04.001.

590 Tsutomu, N., (2002). Geomagnetic storms. *Journal of communications Research Laboratory*, Vol.
591 49, No.3.

592 Turner, N.E., Mitchell, E.J., Knipp, D.J., Emery, B.A., (2006), Energetics of magnetic storms
593 driven by corotating interaction regions: a study of geoeffectiveness, *Geophysical Monograph*
594 *Series 167*, 10.1029/167GM11.

595 Unikrishnan, K., (2008). Comparison of chaotic aspect of magnetosphere under various physical
596 conditions using AE index time series. *Ann. Geophys.*, 26, 941-953, [www.ann-](http://www.ann-geophys.net/26/941/2008)
597 [geophys.net/26/941/2008](http://www.ann-geophys.net/26/941/2008).

598 Unikrishnan, K., Ravindran, S., (2010). A study on chaotic behaviour of equatorial/low latitude
599 ionosphere over indian sub-continent, using GPS-TEC time series, *J. Atmos. Sol. Ter. Phys.*,
600 72, 1080-1089.

601 Valdivia, J.A., Rogan, J., Munoz, V., Gomberoff, L., Klimas, A., Vassiliadis, D., Uritsky, V.,
602 Sharma, S., Toledo, B., Wastaviono, L. (2005). The magnetosphere as a complex system. *Adv.*
603 *Space. Res.*, 35, 961-971.

604 Valdivia, J.A., Sharma, A.S., Papadopoulos, K., (1996). Prediction of magnetic storms by nonlinear
605 models. *Geophysical Research Letters*, 23(21), 2899-2902, doi: 10.1029/96GL02828.

606 Vassiliadis, D., (2006). Systems theory for geospace plasma dynamics, *Rev.Geophys.*, 44, RG2002,
607 doi: 10.1029/2004RG000161.

608 Vassiliadis, D., Klimas, A.J., Valdivia, J.A., Baker, D.N., (1999). The geomagnetic response as a
609 function of storm phase and amplitude and solar wind electric field. *Journal of Geophysical*
610 *Research*, 104(A11), 24957-24976, doi: 10.1029/1999JA900185.

611 Vassiliadis, D., Sharma, A.S., Papadopoulos, K., (1991). Lyapunov exponent of magnetospheric
612 activity from AL time series. *J. GeoPhys. Letts*, Vol. 18, No.8, PP. 1643-1646.

613 Vassiliadis, D.V., Sharma, A.S., Eastman, T.E., Papadopoulou, K., (1990). Low-dimensional
614 chaos in magnetospheric activity from AE time series. *J. GeoPhys.Res.Lett*, 17, 1841-1844.

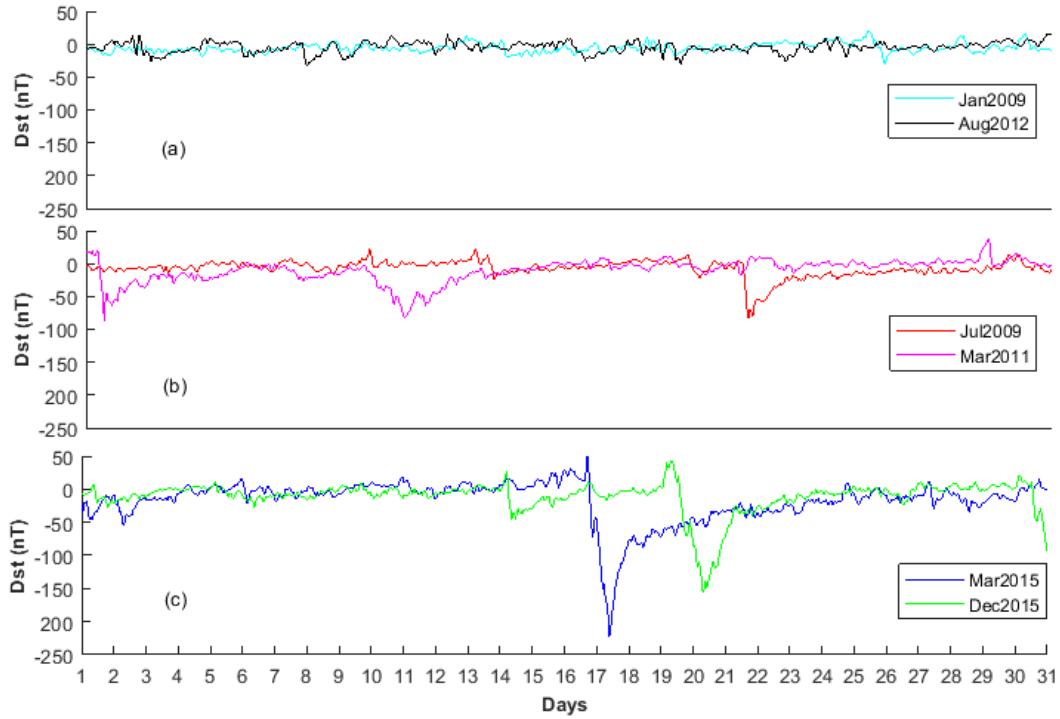
615 Wallot, S., Monster, D., (2018). Calculation of Average Mutual Information (AMI) and False
616 Nearest Neighbours (FNN) for the estimation of embedding parameters of multidimensional
617 time series in MATLAB. *Front. Psychol.* 9:1679, doi: 10.3389/fpsyg.2018.01679.

618 Watari, S., (2017). Geomagnetic storms of cycle 24 and their solar sources, *Earth, Planets and*
619 *Space*, PP: 69:70, doi: 10.1186/s40623-017-0653-z.

620 Wolf, A., Swift, J. B., Swinney, H. L., and Vastano, J. A. (1985). Determining Lyapunov exponents
621 from a time series, *Physica D*, 16, 285–317, doi:10.1016/0167-2789(85)90011-9.

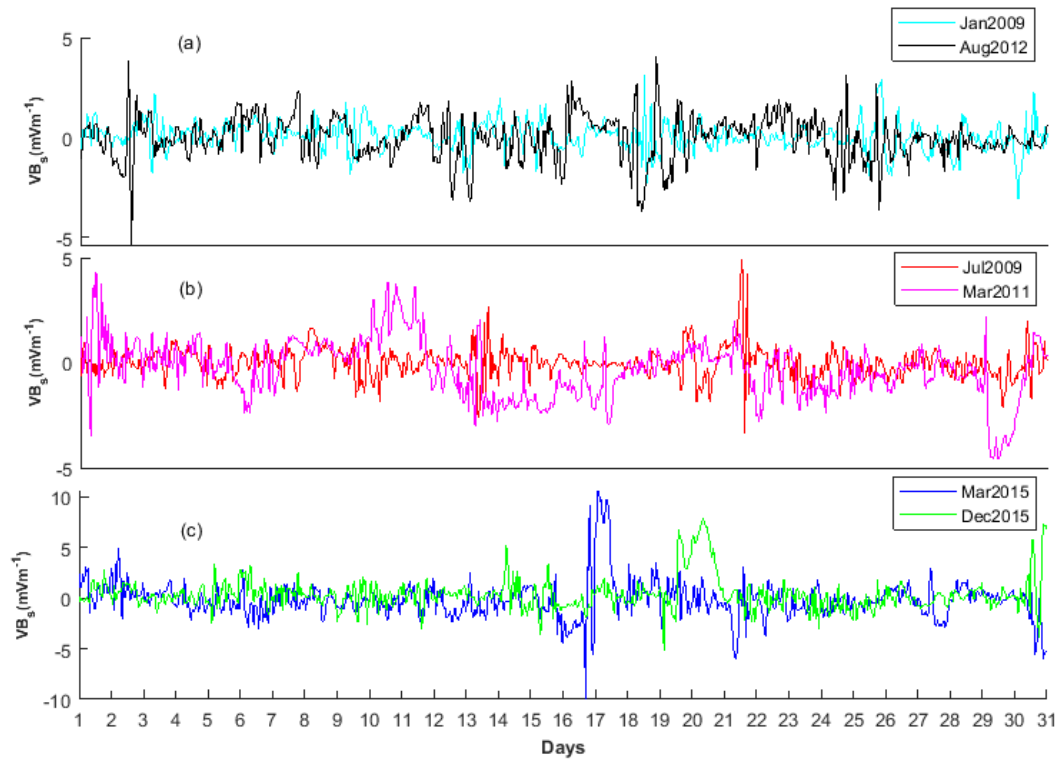
622 Zhang, J., Dere, K.P., Howard, R.A., Bothmer, V., (2002), Identification of solar sources of major
623 geomagnetic storms between 1996 and 2000. *Astrophysical Journal*, 582:520-53.

624



625

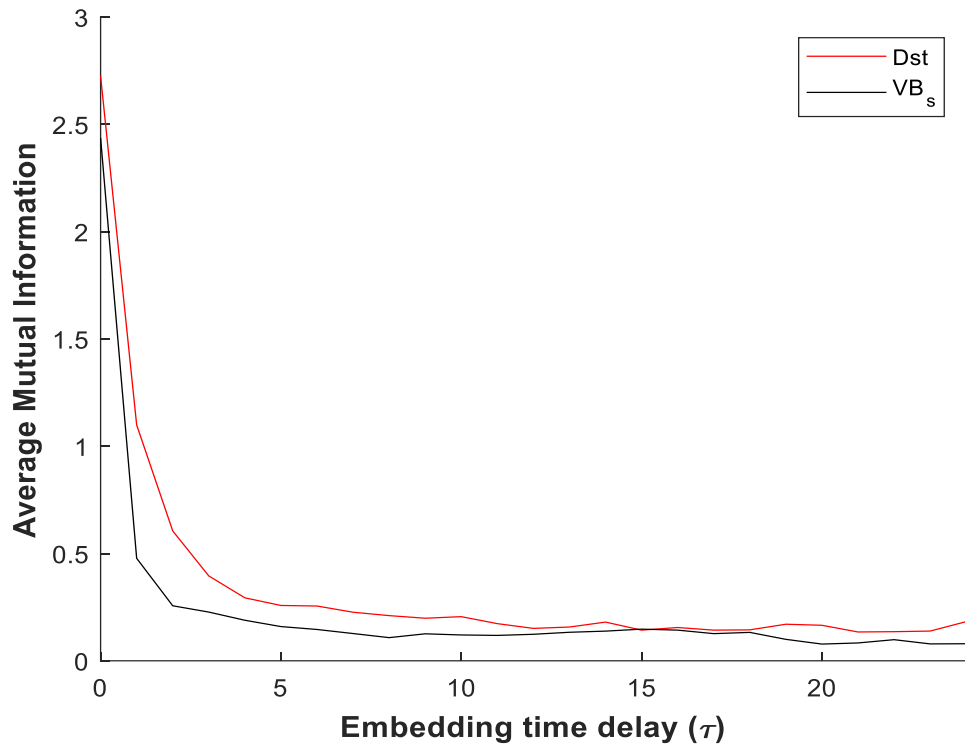
626 Figure 1: Samples of Dst signals classified as (a) Month of Minor, (b) Month of Moderate and (c)
 627 Month of Major geomagnetic storm activity



628

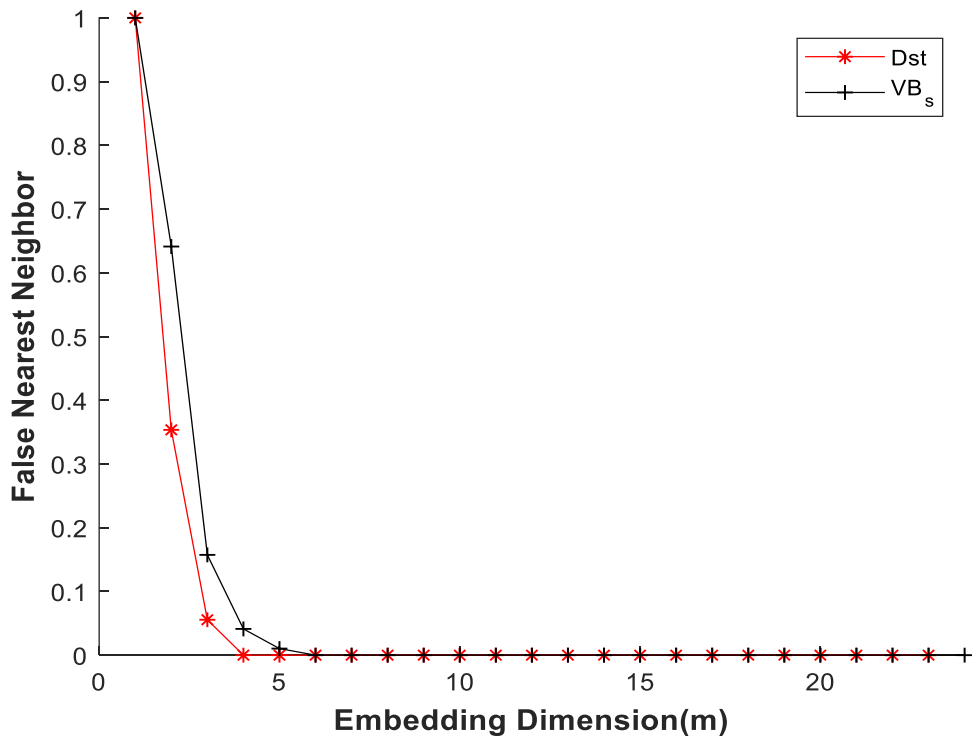
629 Figure 2: Samples of (VB_s) during (a) Month of Minor, (b) Month of Moderate and (c) Month of
 630 Major geomagnetic storm activity.

631



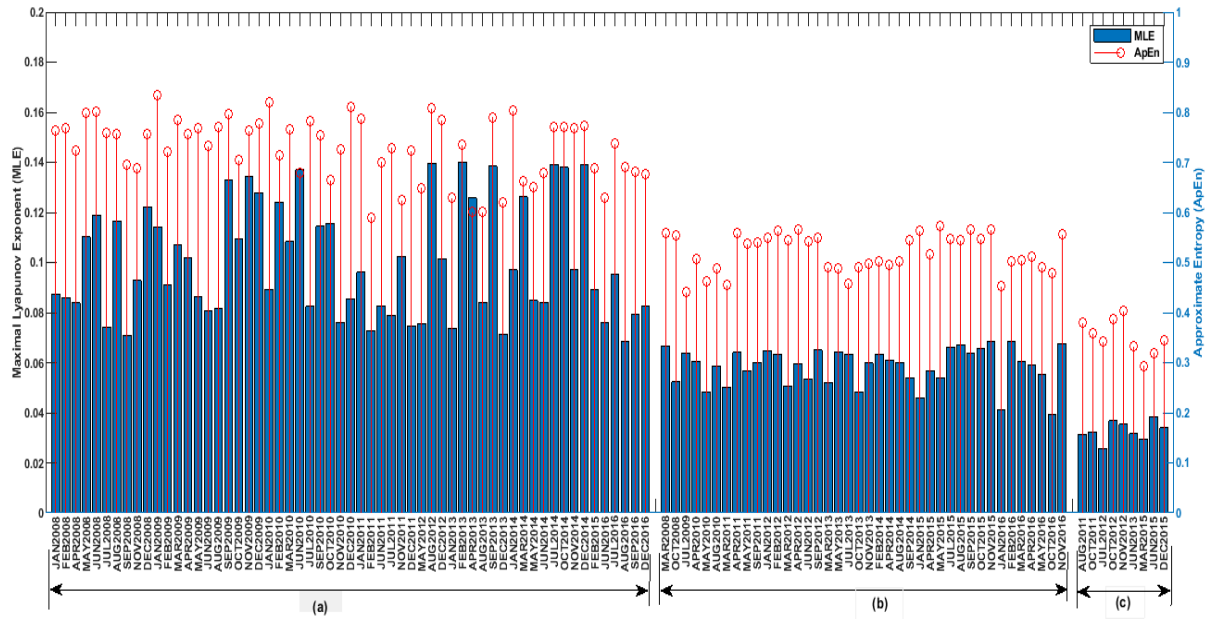
632

633 Figure 3: The plot AMI against embedding time delay (τ)



634

635 Figure 4: The plot of FNN against embedding dimension (m)



636

637 Figure 5: The MLE (bar plot) and ApEn (stem plot) of Dst at: (a) Month of Minor, (b) Month of
 638 Moderate and (c) Month of Major geomagnetic storm activity

639

640

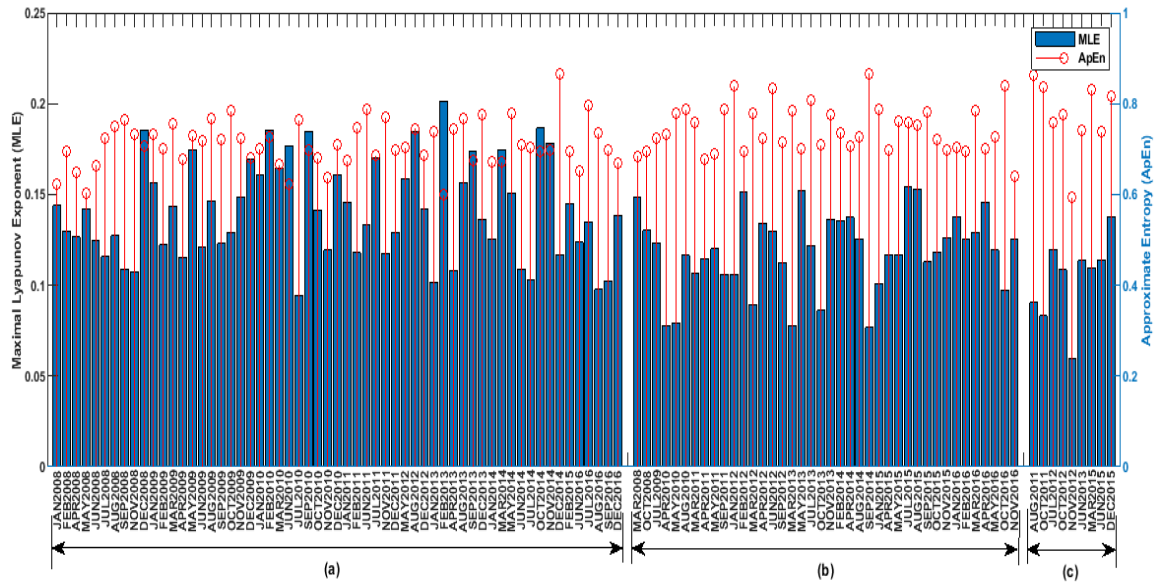
641

642

643

644

645



646

647 Figure 6: The MLE (bar plot) and ApEn (stem plot) of solar wind electric field (VB_S) during: (a)
 648 Month of Minor, (b) Month of Moderate and (c) Month of Major geomagnetic storm activity.

649

650

651

652

653

654

655

656

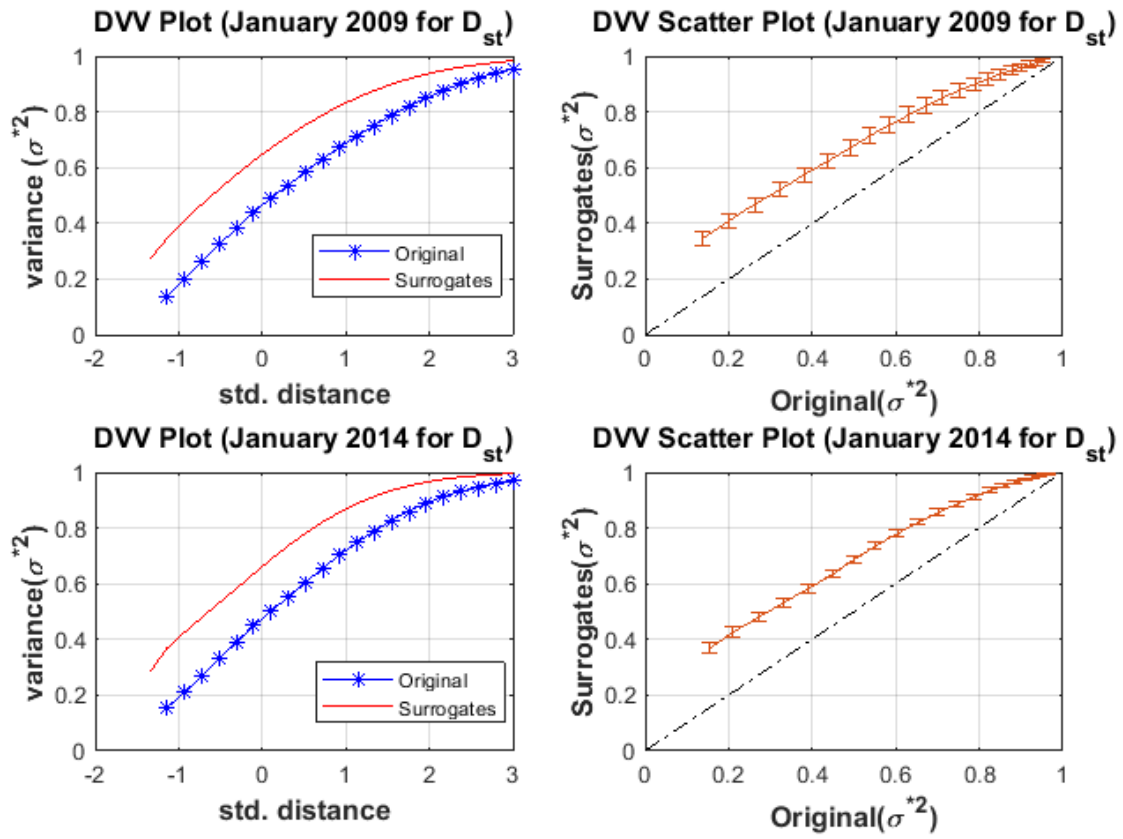
657

658

659

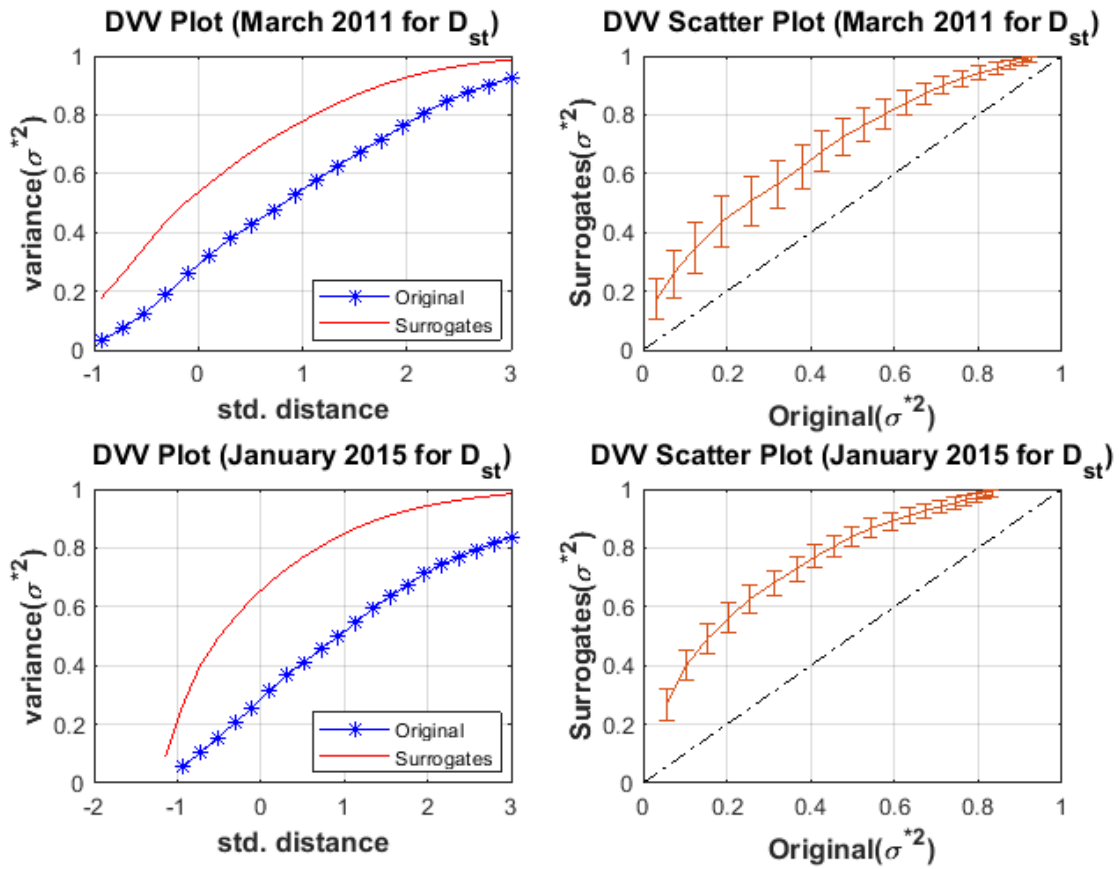
660

661



662

663 Figure 7: The DVV plot and Scatter plot for D_{st} during the month of minor geomagnetic storm
 664 for January 2009 and January 2014.

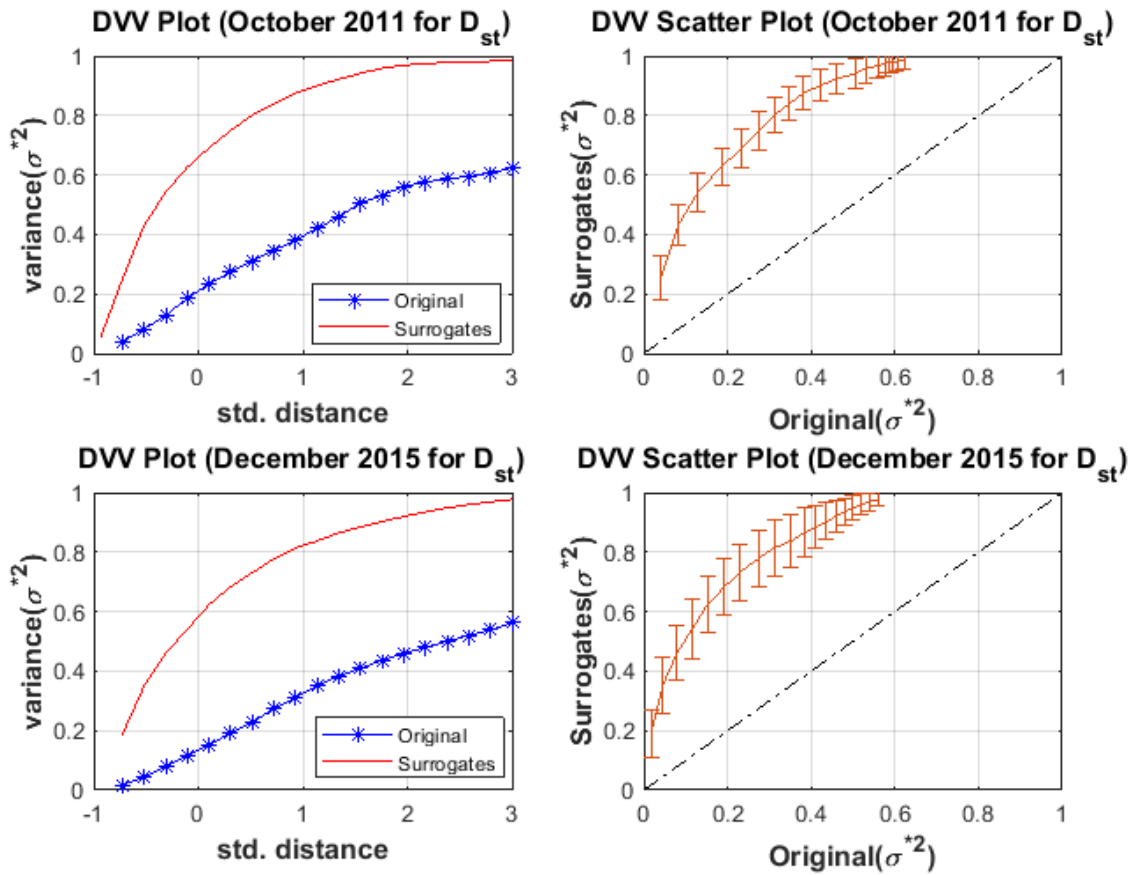


665

666

667 Figure 8: The DVV plot and Scatter plot for D_{st} during the month of moderate geomagnetic storm
 668 for March 2011 and January 2015.

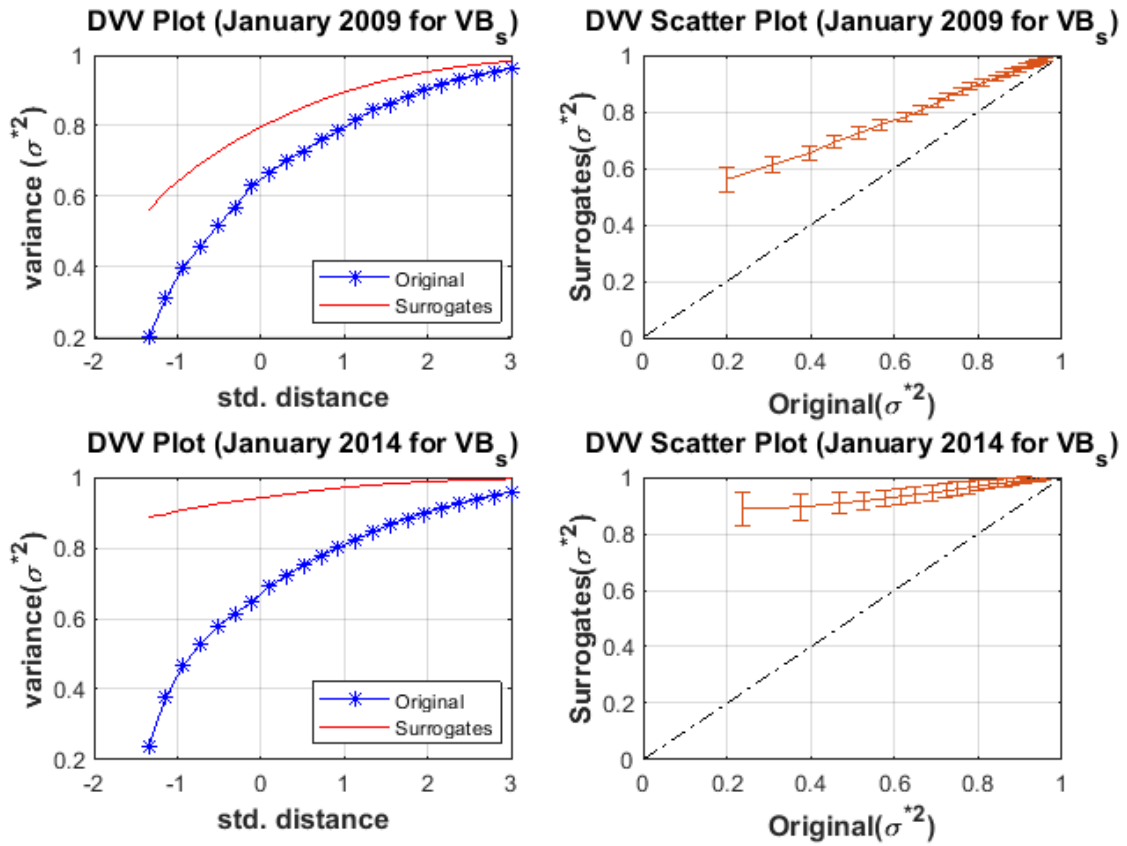
669



670

671 Figure 9: The DVV plot and Scatter plot for D_{st} during the month of major geomagnetic storm
 672 for October 2011 and December 2015.

673

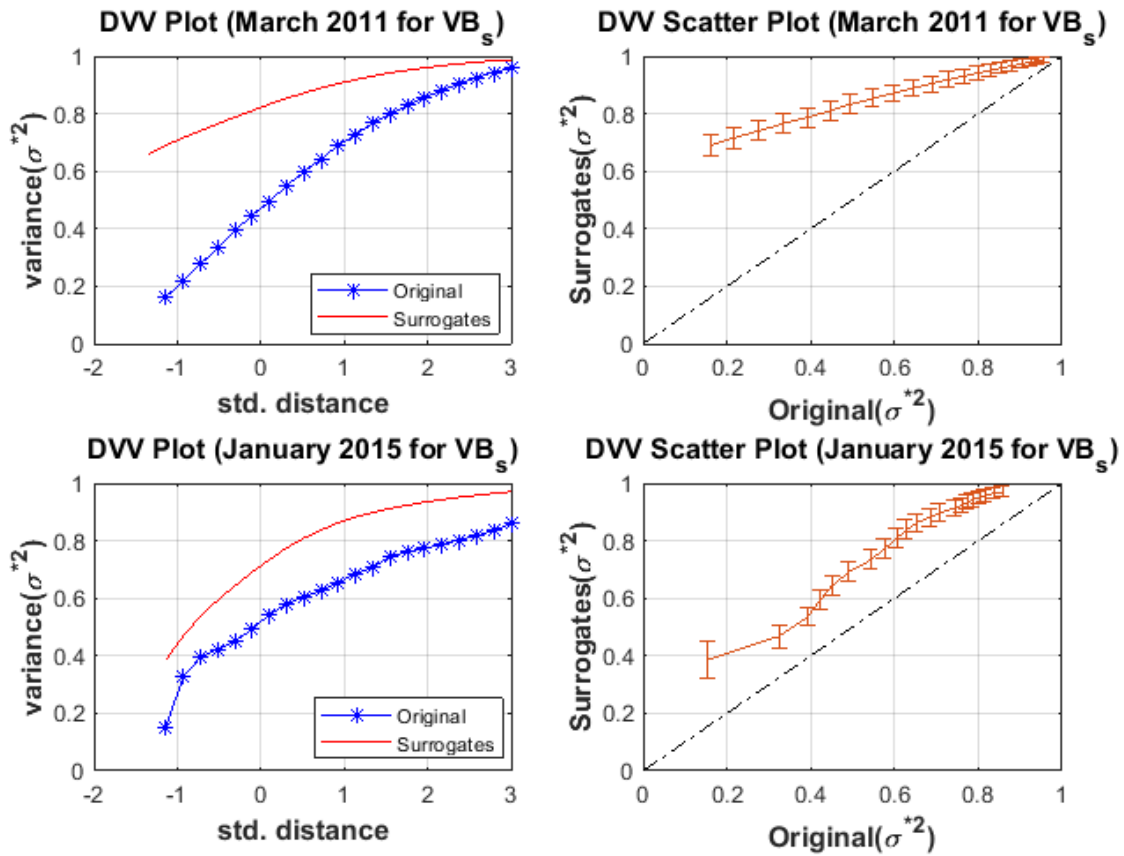


674

675 Figure 10: The DVV plot and Scatter plot for VB_s during the month of minor geomagnetic storm
 676 for January 2009 and January 2014.

677

678

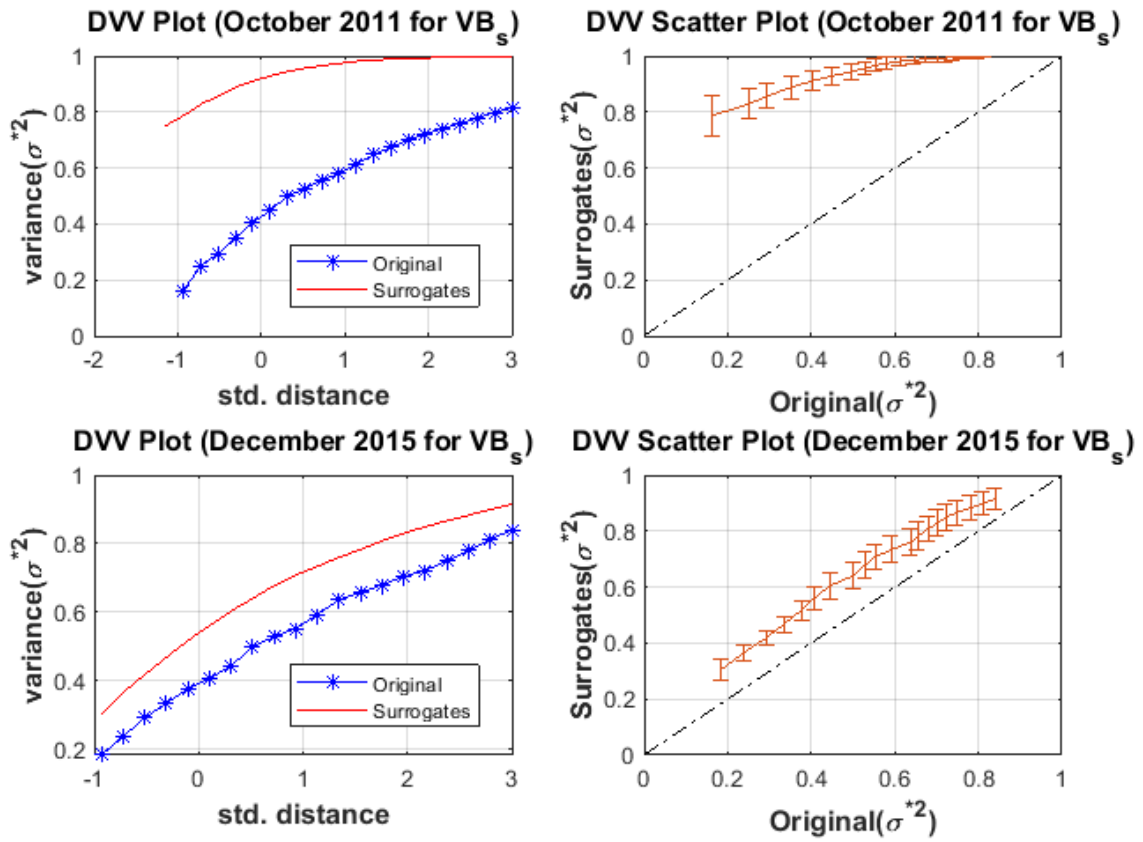


679

680 Figure 11: The DVV plot and Scatter plot for VB_s during the month of moderate geomagnetic
 681 storm for March 2011 and January 2015.

682

683



684

685 Figure 12: The DVV plot and Scatter plot for VB_s during the month of major geomagnetic storm
 686 for October 2011 and December 2015.

687

688

689